Bollettino di Geofisica Teorica ed Applicata Vol. 57, n. 1, pp. 13-30; March 2016
DOI 10.4430/bgta0166

Stress and strain patterns in the Venetian Prealps (north-eastern Italy) based on focal-mechanism solutions

A. Restivo, G. Bressan and M. Sugan

Istituto Nazionale di Oceanografia e di Geofisica Sperimentale - OGS, Centro Ricerche Sismologiche, Udine, Italy

(Received: June 24, 2015; accepted: December 2, 2015)

ABSTRACT Stress and strain patterns are inferred from fault-plane solutions in the seismotectonic domains of the Venetian Prealps, north-eastern Italy. This area represents a peculiar geodynamic sector of the eastern Southalpine Chain, where seismicity marks the indentation between the Adria microplate and the Eurasian plate within a complex tectonic setting. Three distinct seismic districts are investigated (Lessini – L; Pedemontana North and South – PN with PS; and Alpago-Cansiglio - A). Inferences on the stress and strain tensors are based on 55 fault-plane solutions of seismic events that occurred between 1987 and 2014 (magnitude range: 2.6-4.7). Results show that the collision between Adria and the Eurasian plate is generally accommodated by a strike-slip regime. All zones are mainly characterized by focal mechanisms of strike-slip and thrust type, with a wide range of nodal plane orientations, reflecting high crustal structure heterogeneity and a complex pattern of failure planes. The comparison between the principal axes of stress and strain suggests that the L zone is also characterized by a high mechanical strength heterogeneity, which is less pronounced in PN with PS and A zones.

Key words: focal mechanisms, stress and strain inversion, Venetian Prealps, NE Italy.

1. Introduction

This study area represents a peculiar geodynamic sector of the eastern Southalpine Chain (ESC). The seismicity marks the indentation between the Adria microplate and the Eurasian plate (Mantovani *et al*., 1996), which produced a complex tectonic setting. The region was part of the Mesozoic continental margin successively rearranged by the Alpine orogenic events, resulting in different tectonic zones with distinctive seismotectonic characteristics.

Sugan and Peruzza (2011) gather and review seismological databases and seismotectonic literature for the Veneto region and border areas. They divide the region into nine seismic districts. This zonation has been conducted based on structural and geological context, historical and instrumental seismicity, neotectonic and active seismic sources, damaging effects, and seismic regulation. Their work provides a general overview of the earthquakes' space-time distribution, and a more detailed description of the main events of the past and of the potential seismogenic sources in the area.

In the Venetian Prealps there are several geomorphological marks of active deformation (e.g., Benedetti *et al.*, 2000; Galadini *et al.*, 2005; Pola *et al.*, 2014), but rates and geometries of potential seismogenic sources are still uncertain or controversial. Historical earthquakes were documented in the Veneto region since the 8th century (CPTI, 1999, 2004), with destructive events both in the western and eastern sectors [e.g., the 1117 Veronese and 1695 Asolo earthquakes: Rovida *et al.* (2011)]; the instrumental seismicity in this area is quite low, with only a few events equal to or above M_D = 4.0 (Rebez and Renner, 1991) occurring in the period 1977-2013 (Fig. 1), even considering some completeness problems (Gentili *et al.*, 2011).

The focal mechanisms appear essential to understand the present kinematics in such a complex region, where stress heterogeneity could be expected on the basis of the observed broad range of slip plane orientations (Bressan *et al.*, 2003; Viganò *et al.*, 2008; Danesi *et al.*, 2015). Previous studies investigated only portions of this region, using different techniques. The goal of the present study is to infer the stress and strain tensors from fault-plane solutions in the seismotectonic domains of the Veneto area, with the methods of Gephart and Forsyth (1984) and Kostrov (1974). The relative uniformity in strength of the crust is then evaluated by the comparison of stress and strain tensor orientation (Wyss *et al.*, 1992).

To recover the stress and strain patterns in Veneto region focal mechanisms have been calculated for events that occurred in the Lessini (L), Pedemontana North and South (PN with PS) and the Alpago-Cansiglio (A) seismic districts, as defined by Sugan and Peruzza (2011). The area measures about 13,500 km^2 as a whole (Fig. 1). The analysis of focal-mechanism data from the Pedemontana region constitutes an original and essential contribution to understanding the present kinematics in the region. For the L and the A zones, however, our work expands on and upgrades previous quoted results updating the focal-mechanism data set up to 2014.

The number of events needed for a reliable inversion of the stress tensor is closely related to the stress uniformity assumption of the method. The stress tensor inversion of Gephart and Forsyth (1984) is based on the assumption that the stress field is uniform for a given population of focal mechanisms. Albarello (2000) pointed out that "apparent" stress uniformity can arise from a heterogeneous stress field and demonstrated that a stress solution may be found by chance even if the used focal mechanisms belong to different stress domains. The probability of finding a stress field by chance that is compatible with all the focal mechanisms depends on the number of stress domains and also on the number of focal mechanisms attributed to each domain. Therefore, the minimum (and, consequently, the maximum) number of focal mechanisms required for a reliable stress tensor inversion is determined by the stress field uniformity method of Albarello (2000). Within this context, the most important aspect is that the focal mechanisms should be truly representative of the seismotectonic zones, with high-quality solutions and well-constrained planes.

2. Seismotectonic setting

The ESC was formed by Tertiary polyphase compressional evolution and corresponds to the structural belt located to the south of the Periadriatic Lineament (GL to PL to G in Fig. 1). It includes pre-collision, collision (Late Cretaceous–Eocene), and post-collision (Oligocene–Pleistocene) structural systems: the Pre-Adamello structural belt (Late Cretaceous–Eocene), the Dinaric zone

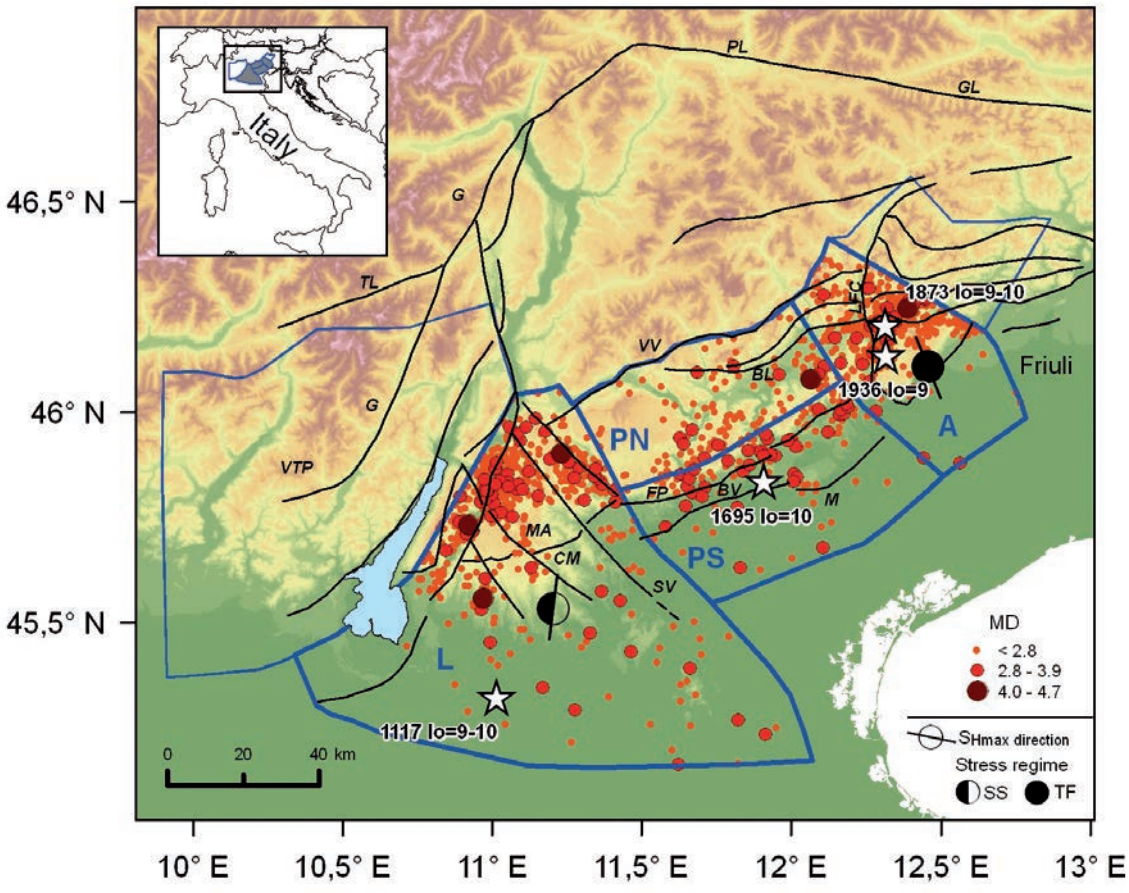

Fig. 1 - Seismicity and stress regime map. Historical seismicity data (white stars) are taken from CPTI11 (Rovida *et al*., 2011); only earthquakes with $M_w \geq 6$ are displayed. M_w is derived from epicentral intensity (I_o) as described at http://emidius.mi.ingv.it/CPTI11/. Instrumental seismicity for the period 1977-2013 is shown (Peruzza *et al*., 2015). Seismic districts as described by Sugan and Peruzza (2011) are superimposed – L: Lessini, PN: Pedemontana North, PS: Pedemontana South, A: Alpago-Cansiglio. Stress and strain data area expressed as maximum horizontal compressive stress (S_{Hmax}) as derived from Viganò *et al*. (2008) and Bressan *et al*. (2003). TF: thrust-fault regime, SS: strike-slip regime. In black, the principal tectonic lineaments are shown on the digital elevation model [schematic representation modified from Castellarin *et al*. (1998)]. GL: Gailtal line, PL: Pusteria line, G: Giudicarie line, TL: Tonale line; VTP: Val Trompia line, CM: Cima Marana thrust; MA: Castel Malera klippen, SV: Schio-Vicenza line, VV: Valsugana thrust, BL: Belluno line, FP: Flessura Pedemontana structural feature, BV: Bassano-Valdobbiadene lineament, M: Montello line, LFC: Longhere-Fadalto-Cadola line.

(Eocene to Chattian/Burdigalian), the Giudicarie (G), Val Trompia (VTP) and Valsugana (VV) belts (Lower-Mid to Upper Miocene), and the Montello (M)–Friuli belt (Messinian–Pleistocene) (Castellarin *et al*., 2006).

Four main structural systems affect the region of interest. The Dinaric NW-SE-trending oldest structural system to the eastern border; the E-W–trending south–verging VV structural system, characterized by thrusts and folds, with a few backthrusts, in the central sector; the NW-SE-trending Schio-Vicenza fault system (SV); and the NNE-SSW Giudicarie structural system (G) in the western sector (Castellarin and Cantelli, 2000).

Fig. 1 shows the main historical events (Rovida *et al*., 2011) together with the instrumental seismicity detected by the Istituto Nazionale di Oceanografia e di Geofisica Sperimentale (OGS)

from 1977 to 2013 (Peruzza *et al.*, 2015) in some seismic districts of the Veneto area, as defined by Sugan and Peruzza (2011). They are mapped on a sketch plot of the major tectonic lineaments in the area (modified from Castellarin *et al.*, 1998). In general, the seismicity concentrates along the front of the Alpine chain, and in the upper crust. A brief description of the structural and seismological characteristics and of the theorized stress pattern for each seismic district follows.

2.1. Lessini (L)

The main structural features in the L district are NW-SE-oriented strike-slip faults. Overthrusts trending NE-SW and ENE-WSW [e.g., Cima Marana (CM)] are also present in the western and northern sector, respectively. The SV line separates the poly-deformed VV system eastwards from the Lessini-Berici-Euganei block. One major historical earthquake struck this district on January 3, 1117 (I_o = IX-X MCS on the Mercalli–Cancani–Sieberg scale), with controversial source hypotheses for it (e.g., Galadini *et al.*, 2005; Guidoboni *et al.*, 2005).

The instrumental seismicity recorded in the 1977-2013 time span is moderate, and it shows only one event with magnitude greater than 4.5 (Pasubio earthquake M_D = 4.7, September 13, 1989). For this area, Viganò *et al.* (2008) showed a predominant maximum horizontal compressive stress oriented NNE, compatible with a right-lateral strike-slip reactivation of the faults belonging to the SV system.

2.2. Pedemontana North and South (PN with PS)

The Pedemontana district is bounded by the VV thrust and the external front of the ESC to the north and south, respectively. The zone is characterized by a system of ENE–WSW–trending and south-verging thrusts and folds, with a few backthrusts and NW-SE-oriented vertical faults with a strike-slip component. The Flessura Pedemontana (FP) and the Bassano-Valdobbiadene-Montello (BVM) lineament are the main tectonic features of this area.

The district has been subdivided into two portions, as the southern sector shows an intense uplift marked by geomorphological evidence (Benedetti *et al.*, 2000; Zanferrari *et al.*, 1982).

The largest damaging earthquake in the past occurred on February 25, 1695 (I_o = X MCS), in the area between Bassano del Grappa and Valdobbiadene. The level of seismic activity is low, and the maximum registered magnitude is associated with the October 14, 1980, earthquake (M_D = 4.0). Very few focal mechanisms are available in the literature for this region: they show heterogeneous solutions (Saraò, 2008; Danesi *et al.*, 2015). The main paleo-stress direction is oriented NW-SE, according to Castellarin and Cantelli (2000). The Montello area seems characterized by a thrusting seismic activity on the basal portion of the Montello structure and strike-slip source kinematics on the western edge of the Montello hill (Danesi *et al.*, 2015).

2.3. Alpago - Cansiglio (A)

The A district represents a transition zone between the structural VV system to the west and the E-W-trending tectonic features of Friuli to the east. Stress transfer occurs along the Longhere-Fadalto-Cadola (LFC) tectonic alignment (Costa *et al.*, 1996; Pellegrini and Surian, 1996), where N-S-trending high-angle dipping faults are prevalent.

Two destructive earthquakes occurred in 1873 (I_o = IX–X MCS) and 1936 (I_o = IX MCS). The Cansiglio 1936 earthquake has been interpreted both as a strike-slip event and with an inverse fault mechanism by Peruzza *et al.* (1989) and Sirovich and Pettenati (2004), respectively. The

seismic activity is moderate with respect to the nearby Friuli area to the east. The maximum magnitude between 1977 and 2013 was recorded for the June 9, 2012, earthquake (M_D = 4.3).

Bressan *et al*. (2003) found that focal mechanisms in this region are mainly of thrust type with subsidiary strike-slip and normal faulting events, with a great variety of nodal plane orientations. The resulting maximum compression axis is oriented approximately NNW-SSE.

3. Focal mechanism data set

The seismicity of the Veneto region has been recorded by the seismic network operated by OGS since 1977 (Fig. 1). The completeness magnitude is very variable in space and time due to the evolution of network geometry, instrumental characteristics, and monitoring and processing strategies over time (Gentili *et al*., 2011).

We analysed seismicity in the Venetian Prealps, selecting and re-locating 55 events that occurred in the period from 1987 to 2014 in the A, PN with PS, and L districts. After 1987, the number of seismic stations increased, and the acquisition system changed from analogue to digital (Gentili *et al*., 2011), thus increasing overall data quality.

Hypocentral locations were performed using the Hypoellipse numerical code (Lahr, 1999). The velocity model used for relocation was inferred from geophysical data (Cassinis *et al*., 2003), minimizing the P and S residual travel times. The model consists of four layers below the surface:

Table 1 - Fifty-five relocated seismic events selected for our study, subdivided by seismotectonic district.

ID	Date [dd/mm/yyyy]	Time [hh:mm]	Lat [°N]	Long [°E]	Depth [Km]	GAP	RMS	ERH	ERZ	MD	Location
Area A - 21 events											
01	11/11/1987	05:55	46.17766	12.31900	10.85	101	0.38	1.0	1.9	3.2	PONTE NELLE ALPI
02	18/04/1988	18:35	46.05733	12.20633	11.54	91	0.29	0.7	1.9	3.5	COL VISENTIN
03	12/07/1990	14:52	46.21166	12.49466	10.99	82	0.23	0.5	1.0	3.4	BARCIS
04	13/09/1993	08:52	46.12383	12.37150	13.18	183	0.17	0.5	0.8	2.8	PUOS D'ALPAGO
05	21/06/1994	19:04	46.10866	12.35250	11.41	102	0.31	0.8	1.1	3.1	PUOS D'ALPAGO
06	09/03/1997	04:03	46.07450	12.22316	8.40	77	0.47	0.7	1.4	2.9	COL VISENTIN
07	16/08/1997	20:59	46.15450	12.36000	9.36	59	0.37	0.5	1.1	3.0	PUOS D'ALPAGO
08	30/05/1999	00:51	46.04200	12.31250	11.07	130	0.45	1.0	1.4	3.0	COL VISENTIN
09	03/05/2000	20:16	46.25050	12.34000	11.88	81	0.24	0.5	0.7	2.9	CIMOLAIS
10	06/05/2000	18:52	46.25816	12.34250	12.13	99	0.35	0.7	1.1	3.1	CIMOLAIS
11	27/08/2004	00:10	46.19500	12.39816	10.92	61	0.32	0.7	1.4	3.1	PIEVE D'ALPAGO
12	07/12/2004	02:19	46.06600	12.31066	11.64	89	0.39	0.9	1.5	3.2	COL VISENTIN
13	28/12/2006	14:10	46.13333	12.21333	9.21	67	0.31	0.5	1.9	3.6	BELLUNO
14	07/03/2010	04:27	46.22400	12.49366	12.83	104	0.28	0.5	0.6	3.3	BARCIS
15	11/03/2010	19:30	46.21583	12.49433	12.96	63	0.37	0.6	1.0	3.3	BARCIS
16	15/04/2010	18:44	46.12766	12.36616	13.46	80	0.30	0.6	1.0	3.2	PUOS D'ALPAGO
17	22/11/2010	17:27	46.24233	12.52750	11.21	57	0.29	0.6	1.1	2.6	BARCIS
18	09/06/2012	02:04	46.19600	12.45066	10.46	47	0.25	0.3	0.8	4.3	PIEVE D'ALPAGO

Table 1 - continued.

ID	Date [dd/mm/yyyy]	Time [hh:mm]	Lat [°N]	Long [°E]	Depth [Km]	GAP	RMS	ERH	ERZ	MD	Location
19	24/08/2013	13:59	46.21533	12.51966	10.47	61	0.22	0.4	0.8	3.6	BARCIS
20	12/09/2013	17:00	46.20566	12.51950	11.14	54	0.33	0.5	1.1	2.8	BARCIS
21	31/10/2013	18:46	46.20866	12.47400	12.45	64	0.22	0.4	0.7	3.0	BARCIS
Area PN with PS - 17 events											
22	16/08/1993	12:34	45.74850	11.62017	6.61	108	0.34	0.2	0.3	2.8	MAROSTICA
23	11/03/1994	06:44	45.81633	11.85900	7.30	109	0.44	0.1	0.4	2.9	BASSANO DEL GRAPPA
24	02/07/1999	16:03	46.08317	11.84517	9.45	141	0.46	0.1	0.3	3.0	FELTRE
25	02/10/1999	03:42	45.87750	11.95583	12.44	158	0.47	0.2	0.4	2.9	VALDOBBIADENE
26	15/06/2001	09:00	45.87167	11.63050	12.50	147	0.33	0.1	0.4	2.8	VALSTAGNA
27	10/12/2001	07:58	45.89533	11.74217	13.39	76	0.42	0.1	0.2	3.3	VALSTAGNA
28	26/05/2002	19:37	45.78917	11.67033	10.03	66	0.36	0.2	0.3	3.2	BASSANO DEL GRAPPA
29	29/09/2004	20:10	45.81050	11.89533	10.27	120	0.24	0.2	0.4	2.8	CASTELFRANCO VENETO
30	04/12/2004	22:20	45.91333	11.98000	10.84	97	0.41	0.1	0.2	3.3	VALDOBBIADENE
31	04/12/2004	22:45	45.90583	11.97300	11.06	97	0.35	0.1	0.2	2.9	VALDOBBIADENE
32	04/12/2004	22:47	45.90850	11.98317	9.45	97	0.37	0.1	0.2	3.0	VALDOBBIADENE
33	20/07/2006	22:47	45.63200	11.84417	11.42	77	0.23	0.2	0.7	3.2	S.MARTINO DI LUPARI
34	04/08/2007	00:25	45.98167	12.22317	5.25	54	0.36	0.1	1.9	3.0	VITTORIO VENETO
35	09/11/2009	10:36	45.81700	11.65950	4.54	172	0.13	0.7	4.4	3.2	CONCO
36	06/12/2009	13:39	45.84383	11.83450	9.02	105	0.40	0.6	1.3	3.3	CAVASO DEL TOMBA
37	29/09/2010	05:36	46.05550	11.75233	10.50	53	0.31	0.3	2.7	3.0	FONZASO
38	13/09/2011	18:35	45.90583	12.04450	10.82	56	0.34	0.6	1.6	3.7	VALDOBBIADENE
Area L - 17 events											
39	13/09/1989	21:54	45.87433	11.16517	12.06	96	0.35	0.5	0.4	4.7	LASTEBASSE
40	24/10/1994	23:22	45.96100	11.18267	9.22	56	0.46	0.1	0.3	3.5	CALDONAZZO
41	25/10/1994	15:09	45.95567	11.18933	9.68	78	0.47	0.2	0.2	2.9	CALLIANO
42	10/02/1996	04:02	45.84050	11.15050	17.46	104	0.46	0.2	0.2	3.0	FOLGARIA
43	26/12/1998	19:46	45.80950	11.38300	12.70	99	0.34	0.1	0.3	3.0	ARSIERO
44	26/04/1999	02:53	45.89900	11.14067	5.64	65	0.32	0.2	0.2	3.6	FOLGARIA
45	18/06/2004	08:50	45.78550	11.33033	9.13	117	0.48	0.2	0.2	2.8	ARSIERO
46	18/05/2005	21:41	45.56333	11.39033	11.14	51	0.42	0.1	0.3	3.4	ARZIGNAGO
47	29/06/2007	14:04	45.86550	11.36783	9.55	91	0.37	0.2	0.3	2.8	ROTZO
48	21/10/2010	14:56	45.78783	11.01800	9.75	95	0.21	0.3	0.9	3.0	ALA
49	28/10/2010	20:38	45.69583	10.93733	11.67	64	0.15	0.4	1.5	3.0	MONTE BALDO
50	29/10/2011	04:13	45.72216	10.93866	9.52	51	0.21	0.7	2.5	4.4	MONTE BALDO
51	31/10/2011	22:12	45.70450	10.93083	13.64	61	0.19	0.5	1.4	3.5	MONTI LESSINI
52	31/10/2011	22:34	45.70233	10.93833	13.53	63	0.16	0.6	1.6	3.5	MONTI LESSINI
53	24/01/2012	23:54	45.55183	10.97433	15.70	85	0.18	0.8	1.4	4.2	GREZZANA
54	18/03/2012	15:59	45.78283	10.99783	12.63	47	0.41	0.2	1.0	3.3	ALA
55	26/06/2014	13:24	45.46333	10.99583	16.00	139	0.18	0.7	1.7	3.0	VERONA

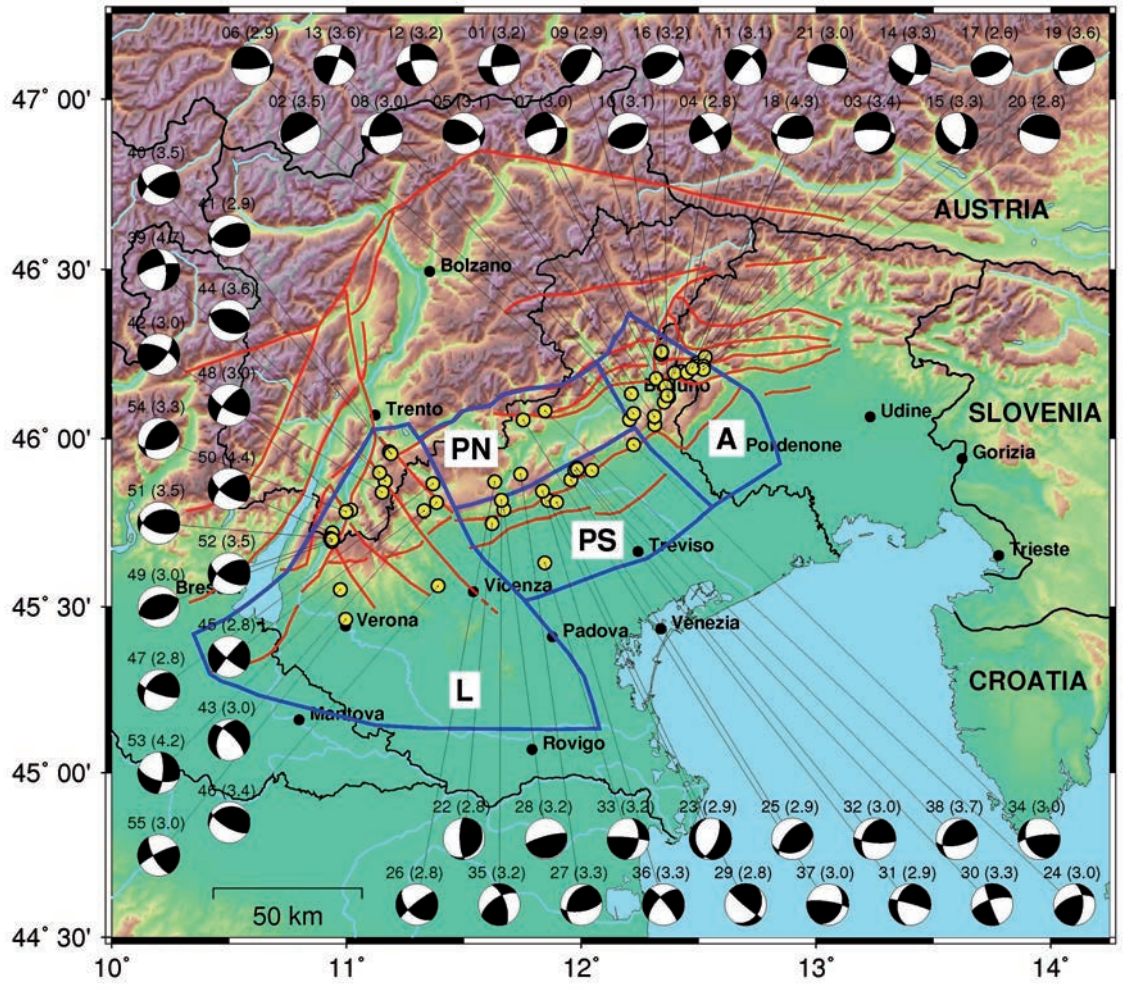

Fig. 2 - Relocated epicentres for 55 selected earthquakes in the Veneto area (yellow dots) and relevant focal-mechanism solutions. Above each mechanism, numbers indicate the event ID as listed in Table 2 and, in brackets, the magnitude of the event. Red lines are the main tectonic lineaments as described in Fig. 1.

0-5 km (Vp: 5.8 km/s, Vp/Vs: 1.83), 5-22 km (Vp: 6.0 km/s, Vp/Vs: 1.80), 22-40 km (Vp: 6.7 km/s, Vp/Vs: 1.76), below 40 km (Vp: 8.0 km/s, Vp/Vs: 1.73).

Table 1 shows the location of the events used in this study, which are plotted in Fig. 2. The average horizontal (ERH) and vertical (ERZ) errors are respectively 0.4 and 1.0 km; coda magnitude (M_D) ranges from 2.6 to 4.7 (September 13, 1989, Pasubio earthquake), with four earthquakes exceeding M_D 4.0; defective angular coverage (GAP) ranges from 47° to 183°.

Focal mechanisms were computed from P-wave first polarities, using the FPFIT code by Reasenberg and Oppenheimer (1985). All the solutions calculated for the Pedemontana districts are new and original results. The Alpago and Lessini areas had been previously analysed by Bressan *et al*. (2003) and Viganò *et al*. (2008), respectively. We extended and updated the available data set of events and P readings for these regions, and reprocessed the data, improving the already published solutions while adding new ones.

The digital seismic recordings were collected and analysed from 1-D and 3-D short-period and broad-band stations of the RSFVG-RSV (Friuli-Venezia Giulia and Veneto) and RSTN (Provincia Autonoma di Trento) seismic networks, as well as from INGV (Istituto Nazionale di Geofisica e Vulcanologia) stations in north-eastern Italy, ZAMG stations in Austria, and ARSO stations in Slovenia. Since 2006, real-time data from these networks have been shared via the Antelope acquisition system used at the CRS (Centro di Ricerche Sismologiche) of OGS. In addition, data from Gräfenberg array stations in Germany were retrieved and analysed for older events. Further phase readings were added from the catalogues of the ISC (International Seismological Centre), INGV and RSFVG.

Input data to FPFIT were weighted with distance, similarly to Viganò *et al*. (2008), but with thresholds at 275 km and 425 km. Lower weight was assigned to higher epicentral distances to account for lower precision readings. In detail, full weight (code 0) was given to records from stations within 275 km of the epicentre, partial weight (1 and 2) to readings from stations between 275 and 425 km and from stations farther than 425 km, respectively. Focal-mechanism solutions for all 55 selected events are listed in Table 2, and they are plotted with reference to the seismic districts in Fig. 2.

Table 2 - Focal-mechanism solutions for selected events used for stress and strain inversion. Plane and axis values expressed in degrees. NP: number of polarity readings used in the solution; NPE: number of polarities incoherent with the calculated solution. QP: quality parameter of the solution based on strike, dip, and rake discrepancy ranges as defined in Reasenberg and Oppenheimer (1985); value A stands for tightly constrained (< 20°) parameters (see text for details). Stress regime as in Zoback (1992); SS: strike-slip faulting (with minor normal or thrust components), NF: normal faulting, NS: predominantly normal faulting with strike-slip component, TF: thrust faulting, TS: predominantly thrust faulting with strike-slip component, U: unknown.

D	NP	NPE	STDR	QP	Stress Regime	First Nodal Plane			Second Nodal Plane			P Axis		T Axis	
						Strike	Dip	Rake	Strike	Dip	Rake	Azim.	Plunge	Azim.	Plunge
Area A - 21 events															
01	49	10	0.52	A	SS	85	85	150	178	60	6	135	17	37	24
02	24	3	0.59	A	U	60	85	100	176	11	27	141	39	341	49
03	29	6	0.61	A	NF	30	30	-150	273	76	-63	214	52	343	26
04	26	1	0.62	A	SS	60	85	10	329	80	175	194	3	285	11
05	40	10	0.54	A	TF	75	50	50	308	54	127	12	2	278	60
06	25	3	0.55	A	TF	85	75	70	320	25	142	191	27	330	56
07	25	7	0.63	A	NS	0	45	-160	256	76	-47	206	42	315	19
08	31	5	0.50	A	U	85	80	130	187	41	15	145	24	32	41
09	23	5	0.47	A	TF	30	70	70	257	28	133	135	22	271	60
10	23	1	0.53	A	TF	60	35	80	252	56	97	337	10	187	78
11	43	5	0.67	A	U	220	85	-40	314	50	-173	169	31	274	23
12	49	9	0.58	A	SS	165	70	-20	262	71	-159	124	28	33	1
13	60	9	0.65	A	SS	20	85	30	287	60	174	150	17	248	24
14	49	9	0.70	A	SS	10	65	-30	114	63	-152	331	38	62	1
15	45	8	0.68	A	NF	135	50	-130	8	54	-53	338	60	72	2
16	42	3	0.52	A	TF	50	60	60	279	41	131	161	10	271	62
17	31	2	0.49	A	TF	60	55	70	272	40	116	164	8	279	72
18	41	8	0.48	A	TF	95	70	120	216	36	36	163	19	43	55

Table 2 - continued.

D	NP	NPE	STDR	QP	Stress Regime	First Nodal Plane			Second Nodal Plane			P Axis		T Axis	
						Strike	Dip	Rake	Strike	Dip	Rake	Azim.	Plunge	Azim.	Plunge
19	43	9	0.48	A	TF	205	30	40	79	71	114	151	23	21	57
20	25	4	0.48	A	TF	105	80	100	240	14	45	186	34	27	54
21	32	7	0.53	A	U	100	85	80	344	11	153	199	39	359	49
Area PN with PS – 17 events															
22	32	5	0.57	A	TF	40	20	130	178	75	77	279	29	70	58
23	52	12	0.62	A	NF	170	30	-120	24	64	-74	323	67	102	18
24	40	9	0.53	A	TS	250	60	140	3	56	37	307	2	215	48
25	42	11	0.51	A	TF	75	35	120	220	60	71	324	13	90	69
26	40	10	0.67	A	U	135	50	170	231	82	40	357	21	101	33
27	54	12	0.54	A	TF	80	65	120	206	38	43	149	15	33	59
28	56	12	0.54	A	TF	75	10	90	255	80	90	345	35	165	55
29	42	11	0.62	A	U	130	85	60	31	30	170	245	33	11	42
30	75	18	0.65	A	SS	160	85	-20	252	70	-175	114	18	208	10
31	48	6	0.59	A	U	285	85	-130	189	40	-8	160	37	46	29
32	70	20	0.52	A	TS	95	75	130	202	42	23	156	20	45	45
33	88	28	0.62	A	U	275	85	140	9	50	7	329	23	224	31
34	71	22	0.56	A	U	155	40	160	261	77	52	19	23	133	44
35	34	3	0.61	A	SS	340	65	30	236	63	152	108	1	199	38
36	52	11	0.70	B	SS	320	80	-150	224	61	-12	186	28	89	13
37	48	9	0.53	A	U	25	35	20	278	79	123	343	26	222	46
38	43	10	0.50	A	TF	80	65	120	206	38	43	149	15	33	59
Area L – 17 events															
39	82	19	0.65	A	SS	50	90	0	320	90	180	185	0	95	0
40	43	4	0.66	A	TS	120	60	140	233	56	37	177	2	85	48
41	41	10	0.54	A	TF	100	45	120	241	52	63	349	4	89	69
42	71	16	0.56	A	SS	40	65	30	296	63	152	168	1	259	38
43	30	3	0.72	A	SS	223	70	-5	315	80	-160	181	17	87	11
44	40	3	0.78	B	SS	40	75	0	310	90	165	356	11	265	11
45	39	5	0.78	A	SS	220	85	10	129	80	175	354	3	85	11
46	34	5	0.73	A	SS	30	90	-15	120	75	-180	345	11	76	11
47	89	18	0.70	A	TS	110	75	130	217	42	23	171	20	60	45
48	49	8	0.83	B	SS	120	70	160	217	71	21	348	1	79	28
49	51	13	0.57	A	TF	70	45	90	250	45	90	340	0	236	90
50	63	3	0.81	A	SS	125	65	150	229	63	28	177	1	86	38
51	44	6	0.74	A	TF	110	55	120	245	45	54	179	6	77	65
52	42	9	0.76	A	TS	120	60	140	233	56	37	177	2	85	48
53	56	1	0.70	A	SS	105	60	-160	5	73	-32	321	34	57	8
54	62	9	0.69	A	TF	75	50	120	213	48	59	144	1	52	67
55	54	12	0.65	A	SS	150	70	170	243	81	20	15	7	108	21

The FPFIT program computed multiple alternative solutions for some smaller-magnitude events. In such cases, we selected the best solution on the basis of a higher STDR (STation Distribution Ratio) parameter and/or lower Misfit value, as defined in Reasenberg and Oppenheimer (1985). In particular, STDR characterizes the quality of the solution by representing data distribution on the focal sphere relative to the radiation pattern, with lower values indicating that many observations lie near nodal planes, therefore standing for a less robust solution than one where STDR>0.5. We also preferred solutions with a more complete and homogeneous data coverage of all the quadrants of the focal sphere and that would better conform with the tectonic lineaments and style known to characterize their epicentral area.

In Table 2, NP represents the number of input polarities, while NPE is the number of polarities in error with the calculated preferred solution; QP is another solution-quality indicator based on computed plane (strike - ϕ, dip - δ) and slip vector (rake - λ) uncertainties as defined in Reasenberg and Oppenheimer (1985): QP = A for $\Delta\phi$ and $\Delta\delta$ and $\Delta\lambda \leq 20°$, QP = B for $20° < \Delta\phi$ and $\Delta\delta$ and $\Delta\lambda \leq 40°$, QP = C for $\Delta\phi$ and $\Delta\delta$ and $\Delta\lambda > 40$. Stress regime is finally defined according to Zoback (1992); U stands for "Undefined".

The minimum and maximum STDR values are 0.47 and 0.83, respectively; 90% of the solutions have an STDR value greater than 0.5 [threshold indicated for robust solutions by Reasenberg and Oppenheimer (1985)]. The STDR average values are 0.70 for the L district, 0.58 for the PN with PS districts and 0.53 for the A area. In terms of QP, 95% of the solutions have maximum quality "A".

Focal mechanisms to be used in the stress tensor inversion were then weighted in the procedure according to both the number of polarities used in computing each solution (NP) and, once more, the STDR parameter (Table 3). Generally, earthquakes with greater magnitude provide a higher number of clear polarity readings so, by using NP as a weighting criterion, higher weight is given to stronger seismic events, which are more representative of the regional stress regime.

Table 3 - Weighting scheme for input data to the stress inversion. District codes (A, PN with PS, and L) as in Sugan and Peruzza (2011). W: weight assigned to a solution based on the number of polarity readings used to compute the focal mechanism (NP) and its STDR value as defined in Reasenberg and Oppenheimer (1985). N: number of events that fall in each weight class.

W	1	2	3	4	5	6
NP	20-40		41-60		>60	
STDR	<0.65	≥0.65	<0.65	≥0.65	<0.65	≥0.65
N (A)	12	0	5	4	0	0
N (PN with PS)	3	1	8	1	3	1
N (L)	0	4	2	6	1	4
N TOT	15	5	15	11	4	5

4. Stress and strain tensor inversion method

The orientation of the principal axes of stress was computed from the inversion of focal-mechanism data using the technique of Gephart and Forsyth (1984). The method determines the orientation of σ_1, σ_2 and σ_3 (maximum, intermediate and minimum stress, respectively) and the

parameter $R = (\sigma_2 - \sigma_1)/(\sigma_3 - \sigma_1)$ as a measure of relative stress magnitudes. The method is based on the assumption that the stress tensor is the same for a given population of focal mechanisms (i.e., even if different types of focal mechanisms are observed in a given space, the tectonic stress tensor is uniform). This condition is fully satisfied if the slip direction on a plane of any focal mechanism is aligned with the direction of the resolved shear stress tensor.

The stress inversion method provides the stress model that minimizes the differences between the calculated and observed slip direction on each focal-mechanism plane. The difference between computed slip and observed slip is evaluated through an angular rotation (misfit) around an arbitrary axis. Therefore, the misfit is the minimum rotation which brings the slip of one of the two nodal planes to match the resolved shear stress tensor, calculated through a grid search, varying systematically the orientation of the principal stresses and the parameter R.

The strain tensor elements ε_{ij} and the principal axes of strain ε_1, ε_2, ε_3 (maximum, intermediate and minimum shortening, respectively) were computed using the relationship (Kostrov, 1974):

$$\varepsilon_{ij} = \frac{1}{2\mu V}\sum_k M_{ij}^k \qquad (1)$$

where μ is the shear modulus, V the crustal volume affected by seismicity and M_{ij}^k the moment tensor of the k-th earthquake. The scalar seismic moment M_o is obtained from the duration magnitude by the relation:

$$\mathrm{Log}M_o = 1.46M_D + 8.83, \text{ with } \sigma_{logM_0} = \pm 0.3 \qquad (2)$$

resulting from the analysis of the Franceschina *et al*. (2006) data set. The value of the shear modulus is assumed to be $3.0 \cdot 10^4$ MPa. The uncertainties related to the computation of the principal axes of strain were calculated following the approach of Wyss *et al*. (1992).

Table 4 - Principal axes of stress. Results of the stress inversion. N is the number of focal mechanisms used in the inversion. F is the minimum average misfit, in degrees. σ_1: maximum compression stress, σ_2: intermediate compression stress, σ_3: minimum compression stress. Azimuth and plunge are expressed in degrees. $R = (\sigma_2 - \sigma_1)/(\sigma_3 - \sigma_1)$.

ZONE	N	F	σ_1		σ_2		σ_3		R
			Azimuth	Plunge	Azimuth	Plunge	Azimuth	Plunge	
A	21	4.3	169	18	281	48	65	36	0.6
PN with PS	17	6.8	322	11	99	75	230	10	0.4
L	17	2.5	159	5	262	68	68	21	0.5

Table 5 - Principal axes of strain. Orientations of the principal axes of strain in the seismotectonic zones. N is the number of the focal mechanisms used in the computation. ε_1: maximum shortening axis, ε_2: intermediate shortening axis; ε_3: mimimum shortening axis. Azimuth and plunge are expressed in degrees.

ZONE	N	ε_1		ε_2		ε_3	
		Azimuth	Plunge	Azimuth	Plunge	Azimuth	Plunge
A	21	160	21	262	28	39	54
PN with PS	17	143	3	49	56	234	34
L	17	202	28	354	59	106	13

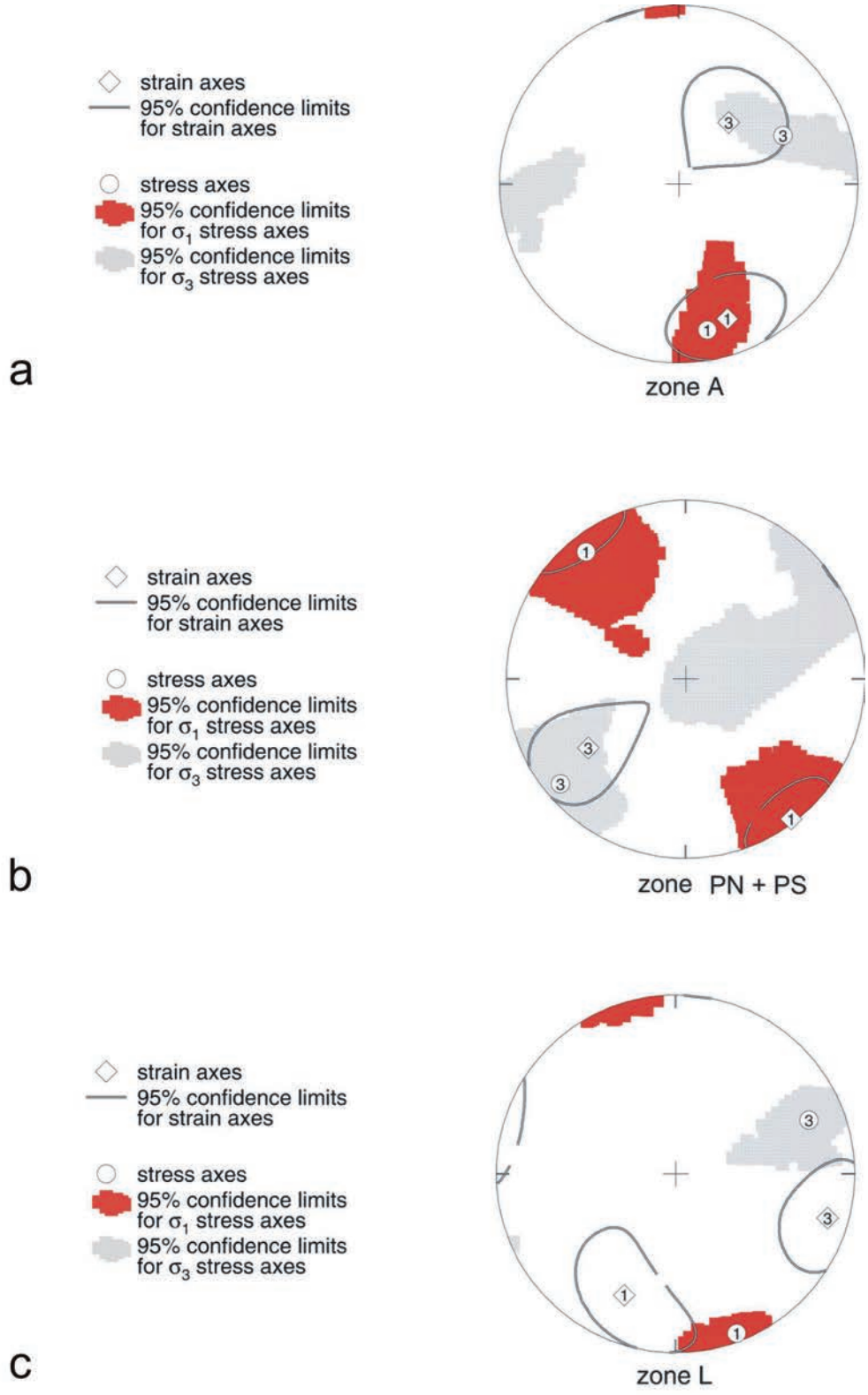

Fig. 3 - Lower hemisphere stereographic projection of the maximum and minimum principal stress and strain axes, with their 95% confidence range: zones A (a), PN with PS (b) and L (c), respectively.

The principal axes of stress and strain retrieved for the A, PN with PS, and L seismotectonic areas are reported in Tables 4 and 5, respectively. The stereographic projections of the maximum and minimum principal stress and strain axes, with the corresponding 95% confidence limits, are shown in Fig. 3 (panels (a), (b), (c), for zone A, zone PN with PS, and zone L, respectively).

5. Discussion

The A area is characterized by a strike-slip stress regime with a relevant reverse component. The stress magnitude ratio (*R*-value) is 0.6. The orientation of the maximum compression stress is about NNW-SSE with 18° plunge. The maximum shortening axis resulting from the strain tensor inversion is oriented about NNW-SSE with 21° plunge. This result is different from and does not confirm the inversion obtained by Bressan *et al.* (2003), where a thrust regime with strike-slip component was found. However, the focal mechanisms of the previous stress inversion were characterized by lower quality, due to a low number of polarities and, in some cases, to poorly constrained planes [see Table 2 in Bressan *et. al* (2003)]. The data set used in the present stress inversion contains instead many new fault-plane solutions, computed from a higher number of first polarities, and having better constrained planes and quality. The PN with PS area is subject to a strike-slip stress regime. The *R* value is 0.4. The maximum compression stress axis is oriented about NW-SE with 11° plunge, and the maximum shortening is horizontal, trending about NW-SE. Finally, the L area is characterized by a strike-slip stress domain, confirming the stress inversion model of Viganò *et al.* (2008). The differences in the orientation of the principal axes of stress and strain (less than 30°) are due to the different data used and to the slightly different areal extent considered here. The obtained *R*-value is 0.5. The maximum compression axis is horizontal and oriented NNW-SSE. The maximum shortening axis is characterized by NNE-SSW trending and 28° plunge.

The stress tensor is considered well resolved when the areas, defined on a stereonet by the 95% confidence limits of σ_1 and σ_3 orientations, do not overlap (Gephart and Forsyth, 1984). The increasing heterogeneity of the stress field causes progressive widening of the stress solution confidence limits and an increase of misfit.

The contours of the σ_1 and σ_3 axes for the 95% confidence limits are clearly separated in all cases. The confidence limits indicate a stable inversion in the A (Fig. 3a) and L (Fig. 3c) zones. They are wider in the case of the PN with PS zone (Fig. 3b), suggesting stress field heterogeneities.

The 95% confidence limits of the principal strain axes appear small everywhere, the axes themselves being well constrained.

The evaluation of the homogeneity of the stress field, based on the width of the confidence limits, has been criticized by Albarello (2000). The author developed a statistical test to check the homogeneity of the stress tensor direction in a volume that works on a set of fault-plane solutions based on a resampling approach. The test recognizes that, although a number of focal mechanisms belong to different stress domains in a heterogeneous volume, a stress solution compatible with them may be found by chance.

It is possible to compute the probability of finding such an erroneous solution for different stress configurations (i.e., partitions of the volume into subdomains or, equivalently, partitions

of the available focal mechanisms into a number of subsets). The configurations for which a low probability is obtained are excluded as unlikely. Homogeneity can be assumed at some level of significance if the only configuration not rejected is the one formed by a unique subdomain.

This approach is very conservative, since it assumes that the stress field is heterogeneous and focal-mechanism data are used to invalidate this hypothesis.

In the test, a fault geometry with compressional and dilatational axes **P** and **T** is assumed to be compatible with a stress field having principal stress axes σ_1 and σ_3 if

$$| \sigma_1 \bullet \mathbf{T} | > | \sigma_1 \bullet \mathbf{P} | \text{ and } | \sigma_3 \bullet \mathbf{T} | < | \sigma_3 \bullet \mathbf{P} | \tag{3}$$

Given N focal mechanisms from an heterogeneous volume including K stress domains, each one responsible for n_i focal mechanisms ($\sum n_i = N$), the probability of finding a stress field compatible with all the focal mechanisms by chance, in the case that M directions are explored, is:

$$P(H_0) = 1 - \left[\prod_{i=1}^{K} \left(1 - 0.5^{N-n_i} \right) \right] \left[\left(1 - 0.5^{N} \right)^{M-K} \right] \tag{4}$$

Such probability depends not only on the number of stress domains but also on the number n_i of focal mechanisms attributed to each of them. Then, a stress configuration is uniquely individuated by a set $\{n_1, n_2, ..., n_K\}$. For example, given 10 focal mechanisms, two of the possible configurations for $K = 3$ are {1,1,8} and {1,4,5}, while the only configuration for $K = 1$ is {10}.

To deal correctly with uncertainties associated with focal-mechanism solutions, the procedure uses a number of artificial samples drawn from the original data set with random resampling. Given L samples, each one including N focal mechanisms from the same heterogeneous volume as above, the probability of finding a stress field compatible with at least Q samples is

$$P' = \sum_{J=Q}^{L} \frac{L!}{J!(L-J)!} P(H_0)^J \left[1 - P(H_0) \right]^{L-J} \tag{5}$$

The procedure involves the following steps:

1 L samples, each of N focal mechanisms, are drawn from the original data set with random resampling;
2. for each sample, a stress field compatible with it is searched for by exploring a grid of M possible solutions;
3. Q is the number of samples for which such a stress field is found;
4. for such Q, the corresponding probability P' of Eq. 5 is computed for every possible stress configuration $\{n_1, n_2, ..., n_K\}$;
5. all the stress configurations for which $P'<0.05$ are excluded as unlikely (i.e., they are excluded at the 5% significance level);
6. the remaining stress configurations $\{n_1, n_2, ..., n_K\}$ are ordered according to the value of K. K_{max} is the maximum K for which a stress configuration exists that cannot be excluded at the 5% significance level. We interpret K_{max} as the degree of heterogeneity of the volume. In particular, if $K_{max} = 1$, the only stress configuration that is not excluded is $\{N\}$ (i.e., all the focal mechanisms in the same subset) and the volume is considered fully homogeneous at the 5% significance level.

The test has been performed using a grid search of 236 directions and a set of 10,000 artificial samples. The results are shown in Table 6, where, in the last column, we report the maximum *K* for which a stress configuration exists that cannot be excluded at the 5% significance level.

Table 6 - Uniformity test. Results of the uniformity test by Albarello (2000). *N*: number of focal mechanisms used in the stress inversion, *M*: number of explored directions; *L*: number of artificial samples including *N* focal mechanisms obtained from the original data set with random resampling; *Q*: artificial samples for which a compatible stress field exist; K_{max}: maximum *K* (number of domains partitioning the volume) for which at least one stress configuration exists that cannot be excluded at the 5% significance level.

ZONE	*N*	*M*	*L*	*Q*	K_{max}
A	21	236	10000	2034	3
PN with PS	17	236	10000	2385	3
L	17	236	10000	10000	1

The homogeneity test resolves that the stress field of the seismotectonic zones A and PN with PS is affected by a low degree of heterogeneity, while is fully homogeneous in the zone L.

The resulting stress domains are *K*=3 {19-1-1} and *K*=3 {15-1-1} for the A and the PN+PS zones, respectively. The homogeneity test indicates a prevailing domain with other negligible ones, each characterized by a single event. The L zone is characterized instead by *K*=1, the only stress domain including all the focal mechanisms. Our stress inversion confirms the stress domain found by Viganò *et al*. (2008), but our data set fully satisfies the homegeneity test for the stress inversion.

The computed strain tensor orientations show that maximum shortening axes are oriented NNW-SSE in zone A, NW-SE in zones PN with PS, while the axis is oriented NNE-SSW in zone L. The spread of the principal strain axis indicates different fault patterns related to different focal mechanisms.

The relative uniformity in strength of the crust can be evaluated by comparing the stress and strain tensor orientations (Wyss *et al*., 1992). If the strength of the crustal volume is uniform, the orientations of the principal axes of stress and strain are similar. If the investigated crust is affected by a dominant fault zone (plane of mechanical weakness), not favourably oriented for failure with respect to the principal axes of stress, slip could occur on it, despite the resolved shear stress being small. In this case, the directions of the principal stress and strain axes differ significantly. However, when comparing stress and strain tensors, it is necessary to consider the different approaches used to determine them (Wyss *et al*., 1992). The stress tensor is the tectonic stress causing earthquakes and is obtained with a fitting process between the resolved shear stress component of the principal stresses and the slip vectors of a population of focal mechanisms. The strain tensor is related instead to the deformations caused by the earthquakes. The weight of focal mechanisms in the stress inversion is related to the quality assigned to each fault-plane solution combined with the number of polarities, while in computing the strain tensor each event is weighted by its seismic moment.

According to Wyss *et al*. (1992), two directions of stress and strain axes will be considered approximately the same if they are within 20°, and their 95% confidence limits are substantially overlapping. This condition is partially fulfilled in the A and PN with PS zones but is not satisfied in zone L, where the difference between the orientation of σ_1 and ε_1 is about 45° and the difference

between the orientation of σ_3 and ε_3 is about 38°.Thus, our results suggest that the L zone is characterized by a mechanically heterogeneous crust, where seismic events occur on differently oriented planes of structural weakness, even if not favourably oriented for slip with respect to the stress tensor, as emerged in Viganò *et al*. (2008).

6. Conclusions

Our results show that the indentation between the Adria microplate and the Eurasian plate is generally accommodated in the Veneto area by a prevalent strike-slip regime.

All subzones are characterized by focal mechanisms of mainly strike-slip and thrust type with a wide range of orientations of the nodal planes, reflecting the heterogeneity of the crustal structure and a complex pattern of failure planes.

District A shows a strike-slip stress regime with a relevant reverse component, where the maximum compression stress and the maximum shortening axes are oriented NNW-SSE. The PN with PS area is subject to a strike-slip stress regime, with the maximum compression stress and the maximum shortening axes being oriented NW-SE. A strike-slip stress domain also characterizes the L area. Here the maximum compression axis is horizontal and oriented NNW-SSE, and the maximum shortening axis is trending NNE-SSW.

The stress homogeneity test indicates that the stress field is uniform in the seismotectonic zone L and slightly heterogeneous in the seismotectonic zones A and PN with PS. The test also confirms that the number of focal mechanisms used is satisfactory for stable stress inversions.

The comparison between the principal axes of stress and strain suggests that the L zone is characterized by heterogeneous crustal strength. The mechanical heterogeneity is less pronounced in zones PN with PS and A.

Acknowledgements. This research was financially supported by the Regione Veneto and the Regione Autonoma Friuli Venezia Giulia. We thank P.L. Bragato, P. di Bartolomeo, and L. Peruzza for the technical support and scientific discussion. We are thankful to two anonymous reviewers whose comments and suggestions improved this paper.

REFERENCES

Albarello D.; 2000: *A resampling approach to test stress-field uniformity from fault data*. Geophys. J. Int.,**140**, 535-542.

Benedetti L., Tapponnier P., King G.C.P., Meyer B. and Manighetti I.; 2000: *Growth folding and active thrusting in the Montello region, Veneto, northern Italy*. J. Geophys. Res., **105**, 739-766.

Bressan G., Bragato P.L. and Venturini C.; 2003: *Stress and strain tensors based on focal mechanisms in the seismotectonic framework of the Friuli–Venezia Giulia region (north-eastern Italy)*. Bull. Seism. Soc. Am., **93**, 1280-1297.

Cassinis R., Scarascia S. and Lozej A.; 2003: *The deep crustal structure of Italy and surrounding areas from seismic refraction data. A new synthesis*. Boll. Soc. Geol. It., **122**, 365-376.

Castellarin A., Vai G.B. and Cantelli L.; 2006: *The Alpine evolution of the Southern Alps around the Giudicarie faults: A Late Cretaceous to Early Eocene transfer zone*. Tectonophysics, **414**, 203-223.

Castellarin A. and Cantelli L.; 2000: *Neo-Alpine evolution of the Southern Eastern Alps*. J. Geodynamics, **30**, 251-274.

Castellarin A., Selli L., Picotti V. and Cantelli L.; 1998: *La tettonica delle Dolomiti nel quadro delle Alpi meridionali orientali*. Memorie della Società Geologica Italiana, **53**, 133-143.

Costa V., Doglioni C., Grandesso P., Masetti D., Pellegrini G.B. and Tracanella E.; 1996: *Note illustrative del Foglio 063 BELLUNO*. Servizio Geologico d'Italia, Istituto Poligrafico e Zecca dello Stato, Roma, 74 pp.

CPTI Working Group (Boschi E., Gasperini P., Valensise G., Camassi R., Castelli V., Stucchi M., Rebez A., Monachesi G., Barbano M.S., Albini P., Guidoboni E., Ferrari G., Mariotti D., Comastri A. and Molin D.); 1999: *Catalogo Parametrico dei Terremoti Italiani*. ING, GNDT, SGA, Bologna, 92 pp.

CPTI Working Group; 2004: *Catalogo Parametrico dei Terremoti Italiani, vers. 2004 (CPTI04)*. INGV, last access December 2011.

Danesi S., Pondrelli S., Salimbeni S., Cavaliere A., Serpelloni E., Danecek P., Lovati S. and Massa M.; 2015: *Active deformation and seismicity in the Southern Alps (Italy): The Montello hill as a case study*. Tectonophysics, **653**, 95-108, doi.org/10.1016/j.tecto.2015.03.028.

Franceschina G., Kravanja S. and Bressan G.; 2006: *Source parameters and scaling relationships in the Friuli-Venezia Giulia (north-eastern Italy) region*. Phys. Earth Planet. Inter., **154**, 148-167.

Galadini F., Poli M.E. and Zanferrari A.; 2005: *Seismogenic sources potentially responsible for earthquakes with M ≥6 in the eastern Southern Alps (Thiene-Udine sector, NE Italy)*. Geophys. J. Int., **161**, 739-762.

Gentili S., Sugan M., Peruzza L. and Schorlemmer D.; 2011: *Probabilistic completeness assessment of the past 30 years of seismic monitoring in north-eastern Italy*. Phys. Earth Planet. Inter., **186**, 81–96.

Gephart J.W. and Forsyth D. W.; 1984: *An improved method for determining the regional stress tensor using earthquake focal mechanism data: application to the San Fernando Earthquake sequence*. J. Geophys. Res., **89,** 9305-9320.

Guidoboni E., Comastri A. and Boschi E.; 2005: *The "exceptional" earthquake of 3 January 1117 in the Verona area (northern Italy): a critical time review and detection of two lost earthquakes (lower Germany and Tuscany)*. J Geophys. Res., **110**, B12309, doi: 10.1029/2005JB003683.

Kostrov B.V.; 1974: *Seismic moment and energy of earthquakes and seismic flow of rocks*. Izv. Acad. Sci. USSR Phys. Solid Earth, Engl. Transl., **1**, 23-44.

Lahr J.C.; 1999, revised 2012: *HYPOELLIPSE: a computer program for determining local earthquake hypocentral parameters, magnitude, and first-motion pattern*. U.S.G.S. Open File Rep. 99–23, version 1.1, 119 pp. and software, < http://pubs.usgs.gov/of/1999/ofr-99-0023/>.

Mantovani E., Albarello D., Tamburelli C. and Babbucci D.; 1996: *Evolution of the Tyrrhenian basin and surrounding regions as a result of the Africa-Eurasia convergence*. J. Geodynamics, **21**, 35-72.

Pellegrini G.B. and Surian N.; 1996: *Geomorphological study of the Fadalto landslide, Venetian Prealps, Italy*. Geomorphology, **15**, 337-350.

Peruzza L., Iliceto V. and Slejko D.; 1989: *Some seismotectonic aspects of the Alpago-Cansiglio area (N.E. Italy)*. Boll. Geof. Teor. Appl., **31**, 63-75.

Peruzza L., Garbin M., Snidarcig A., Sugan M., Urban S., Renner G. and Romano A.; 2015: *Quarry blasts, underwater explosions, and other dubious seismic events in NE Italy from 1977 to 2013*. Boll. Geof. Teor. Appl., **56**, 437-459.

Pola M., Gandin A., Tuccimei P., Soligo M., Deianas R., Fabbri P. and Zampieri D.; 2014: *A multidisciplinary approach to understanding carbonate deposition under tectonically controlled hydrothermal circulation: A case study from a recent travertine mound in the Euganean hydrothermal system, northern Italy*. Sedimentology, **61**, 172–199.

Reasenberg P., Oppenheimer D.; 1985: *FPFIT, FPPLOT and FPPAGE: Fortran computer programs for calculating and displaying earthquake fault-plane solutions*. Open-File Rep. 85-739, U.S.G.S., Menlo Park, 109 pp.

Rebez A. and Renner G.; 1991:. *Duration magnitude for the north-eastern Italy seismometric network*. Boll. Geof. Teor. Appl., **33,** 177–186.

Rovida A., Camassi R., Gasperini P. and Stucchi M. (eds.); 2011: *CPTI11, the 2011 version of the Parametric Catalogue of Italian Earthquakes*. Milano, Bologna, <http://emidius.mi.ingv.it/CPTI>.

Saraò A.; 2008: *Focal mechanisms of NE Italy and surroundings (1928-2008)*. Rapporti Interni, Istituto Nazionale di Oceanografia e di Geofisica Sperimentale - OGS, Dipartimento Centro di Ricerche Sismologiche, OGS-143/2008/CRS-20, Trieste, Italia, 75 pp.

Sirovich L. and Pettenati F.; 2004: *Source inversion of intensity patterns of earthquakes: a destructive shock in 1936 in northeast Italy*. J. Geophys. Res., **109**, B10309, 1-10.

Sugan M. and Peruzza L.; 2011: *Distretti sismici del Veneto*. Boll. Geofis. Teor. Appl., **52**, suppl., s3-s90, doi: 10.4430/bgta0057.

Viganò A., Bressan G., Ranalli G. and Martin S.; 2008: *Focal mechanism inversion in the Giudicarie–Lessini seismotectonic region (Southern Alps, Italy): Insights on tectonic stress and strain*. Tectonophysics, **460**, 106-115.

Zanferrari A., Bollettinari G., Carobene L., Carton A., Carulli G.B., Castaldini D., Cavallin A., Panizza M., Pellegrini G.B., Pianetti F. and Sauro U.; 1982: *Evoluzione neotettonica dell'Italia nord-orientale*. Memorie di Scienze Geologiche, **35**, 355-376.

Zoback M.L.; 1992: *First- and second-order patterns of stress in the lithosphere: the world stress map project*. J. Geophys. Res., **97**, 11703-11728.

Wyss M., Liang B., Tanigawa W. R. and Wu X.; 1992: *Comparison of orientations of stress and strain tensors based on fault plane solutions in Kaoiki, Hawaii*. J. Geophys. Res., **97**, 4769-4790.

Corresponding author: Andrea Restivo
Centro Ricerche Sismologiche, Istituto Nazionale di Oceanografia e di Geofisica Sperimentale
Via Treviso 55, 33100 Udine, Italy
Phone: +39 040 2140123; fax: +39 0432 522474; e-mail: arestivo@inogs.it